CONF-8906270--3

DE90 008404

CALCULATING COHERENT PAIR PRODUCTION WITH MONTE CARLO METHODS

C. Bottcher and M. R. Strayer
Physics Division
Oak Ridge National Laboratory
Oak Ridge, TN 37831

DISCLAIMER

This report was prepared as an account of work sponsored by an agency of the United States Government. Neither the United States Government nor any agency thereof, nor any of their employees, makes any warranty, express or implied, or assumes any legal liability or responsibility for the accuracy, completeness, or usefulness of any information, apparatus, product, or process disclosed, or represents that its use would not infringe privately owned rights. Reference herein to any specific commercial product, process, or service by trade name, trademark, manufacturer, or otherwise does not necessarily constitute or imply its endorsement, recommendation, or favoring by the United States Government or any agency thereof. The views and opinions of authors expressed herein do not necessarily state or reflect those of the United States Government or any agency thereof.

to be published in

Proceedings of

Summer School of Computational Atomic
and Nuclear Physics
Sewanee, Tennessee
June 26-July 7, 1989

"The submitted manuscript has been authored by a contractor of the U.S. Government under contract No. DE-AC05-84OR21400. Accordingly, the U.S. Government retains a nonexclusive, royalty-free license to publish or reproduce the published form of this contribution, or allow others to do so, for U.S. Government purposes."

MASTER

DISTRIBUTION OF THIS DOCUMENT IS UNLIMITED

CALCULATING COHERENT PAIR PRODUCTION WITH MONTE CARLO METHODS

C. Bottcher and M. R. Strayer

Physics Division, Oak Ridge National Laboratory

Oak Ridge, TN 37831

ABSTRACT

We discuss calculations of the coherent electromagnetic pair production in ultra-relativistic hadron collisions. This type of production, in lowest order, is obtained from tree diagrams which contain two virtual photons. We discuss simple Monte Carlo methods for evaluating these classes of diagrams without recourse to involved algebraic reduction schemes.

1. INTRODUCTION

In this lecture we shall address the question of pair production from classical time-dependent electromagnetic fields. These types of fields are present in the peripheral ultrarelativistic collisions of heavy nuclei [1,2]. Because of the possible coherence in the field, it is speculated that relatively large fluxes of exotic particles may be produced. Such particles include μ and τ pairs,[3,4,5], magnetic monopoles

[6], W-pairs, b-quark pairs, and possibly the Higgs [7,8]. Most of these studies address colliding beams of heavy nuclei at energies per nucleon in the range $3-10^3$ GeV, corresponding to suggested experiments at the AGS, CERN, the proposed RHIC facility at Brookhaven, and possibly the SSC.

Out of these speculations arise a series of questions:

- In view of the interest in dilepton production and J/ψ suppression as a diagnostic of the formation of the quark-gluon plasma, it is important to know whether electromagnetic pair production exhibits features which clearly distinguish it from hard hadronic processes.

- Pairs of W bosons have not yet been produced in laboratory collisions. The Z^4 scaling implicit in the coherent production of these particles may amplify cross section yields sufficiently to be of interest experimentally. Simple calculations suggest that the processes for producing W-pairs are also candidates for producing the Higgs. Thus it may be possible to use heavy-ion machines to search for the Higgs.

- Many of the properties of vector mesons have emerged from the Drell-Yan measurements of electron pair production [9,10]. However, there are anomalies in this analysis which have recently been resolved with a more careful consideration of the hadronic current matrix elements [11,12].

Concerning the coherent production of μ and τ pairs perturbatively, other calculations of cross sections have been performed using the Weizsäcker-Williams

approximation [4,8]. However, this approximation may not always work, since the constraint that the photons must be *on-shell* is not always realizable; an example is the case where the virtual photons carry an explicit transverse momentum [12]. Furthermore, the coherent production of pairs from nuclei is a collective process which is very different than that arising from the collision of point charges. Nucleons in nuclei move at high velocities and carry a large momentum. Form factors control the coupling of these nucleons to photons, and the strength of this coupling regulates the magnitude of the pair cross section. Thus, nuclear and nucleon electromagnetic form factors must be included in these calculations.

Pair production in heavy-ion collisions is nonperturbative at high energies. It is plausible that the introduction of nucleon form factors may regularize the perturbation theory order by order. Thus as noted in Ref. [11,12], Feynman perturbation theory becomes an efficient tool to address details of the hadron-photon couplings and their effect on the lepton cross sections. Calculations in this framework for electron–positron pairs demonstrate a substantial yield at large pair invariant masses and transverse momenta, where equivalent photon approximations are invalid.

In comparing computation to experiment, it is important to understand the experimental constraints placed on the data. The Monte Carlo algorithms discussed in this talk have the advantage that complicated constraints on the reaction phase space can be dealt with in a straightforward manner. We shall apply these methods to calculate cross sections for a variety of complex experiments as follows: anoma-

lous $e^{\pm}$ production in 17 GeV $\pi^- p$ collisions, and μ and τ lepton production in ultrarelativistic collisions of heavy nuclei.

2. SEMICLASSICAL THEORY

Formally, we employ a semiclassical treatment of pair production wherein the leptons are coupled to the classical electromagnetic four-potentials of the colliding nuclei. The source currents are the Lorentz-boosted charge distributions of the colliding ions. In the limit of structureless point charge nuclei, these potentials are the retarded Liénard-Wiechert interactions. However, it is clear from general arguments that the electromagnetic coupling of μ and τ pairs to protons in nuclei depends on the nucleon currents and form factors in each ion. In our present calculations, we are primarily concerned with peripheral heavy-ion collisions, and we construct classical four-vector potentials employing phenomenological nuclear currents and form factors which fit elastic electron scattering data from nuclei.

The formulation of electromagnetic pair production used here is based on the Lagrangian density for the coupling of the classical electromagnetic four-vector potential to the lepton fields given by

$$\mathcal{L}_{int}(x) = -\overline{\Psi}(x)\gamma_\mu\Psi(x)A^\mu(x) \ . \tag{1}$$

This Lagrangian conserves lepton number [2], and we treat the production of electrons, muons, and tauons as occurring independently. The equations of motion for lepton state vectors is obtained from (1) using variational methods. We use a semiclassical action corresponding to a time-dependent *many-lepton* state $\Phi(t)$,

$$\mathcal{S} = \int d^4x < \Phi(t) \mid : \mathcal{L}_0(x) + \mathcal{L}_{int}(x) : \mid \Phi(t) > \ , \tag{2}$$

where the normal ordering is with respect to a reference state, and where $\mathcal{L}_0$ is the usual noninteracting fermion Lagrangian,

$$\mathcal{L}_0(x) = \overline{\Psi}(x)[\gamma_\mu i\partial^\mu - m]\Psi(x) \ . \tag{3}$$

In (2), the dynamical coordinates which are varied to make the action stationary are the parameters labeling the state vector $\Phi(t)$. We additionally assume that the initial state vector corresponds to a single Slater determinant, $\mid O >$,

$$\lim_{t \to -\infty} \mid \Phi(t) > \to \mid O > \ . \tag{4}$$

Since we shall only consider pair production out of the vacuum, we choose $\mid O >$ as the vacuum state, which we also identify as the reference state for the ordering in (2). By construction, we have a well-defined initial Hamiltonian with a corresponding complete and orthonormal set of single-particle states, $\chi_q^{(+)}$ and $\chi_q^{(-)}$, satisfying

$$H_0 \mid \chi_q^{(\pm)} > = E_q^{(\pm)} \mid \chi_q^{(\pm)} > \tag{5}$$

where

$$E_q^{(\pm)} = \pm(m + \vec{q}^{\,2})^{1/2} \tag{6}$$

and

$$H_0 = \vec{\alpha} \cdot \vec{p} + m\alpha_0. \tag{7}$$

Since the above model results in rules that are different than the usual Feynman diagrams for two-photon processes, we find it expedient to norm our states as follows,

$$\sum_q \mid \chi_q^{(+)} >< \chi_q^{(+)} \mid + \mid \chi_q^{(-)} >< \chi_q^{(-)} \mid = 1 \ ,$$

$$< \chi_q^{(i)} \mid \chi_p^{(j)} > = \delta_{q,p}\delta_{i,j} \ . \tag{8}$$

With this choice of reference state, the states $\mid \chi^{(+)} >$ and $\mid \chi^{(-)} >$ are single-particle and single- antiparticle states, respectively. The dynamics governing the time evolution of the states in (2) is unitary, and given by

$$\mid \Phi(t) >= K(t, -\infty) \mid O >, \tag{9}$$

where $KK^\dagger = K^\dagger K = 1$. There are several important consequences of these assumptions. Equations (4) and (9) guarantee that the state Φ is at all times a representation of a single Slater determinant, and equations of motion can be cast into the form

$$H(x)K(t,t') = i\partial_t K(t,t'), \tag{10}$$

where

$$H(x) = H_0(x) + H_{int}(x),$$

$$H_{int}(x) = \gamma_0 \not{A}(x) \tag{11}$$

$$= -\vec{\alpha} \cdot \vec{A}(x) + A_0(x) \ .$$

With the above-noted assumptions, all orders of processes can be obtained from the solutions to (10). In particular, those solutions which are perturbative in H_{int} can be expressed as the series

$$K(t,\infty) = K_0(t,-\infty) + (-i)\int_{-\infty}^{t} d\tau K_0(t,\tau)H_{int}(\tau)K_0(\tau,-\infty) + (-i)^2\int_{-\infty}^{t} d\tau \int_{-\infty}^{\tau} d\tau' K_0(t,\tau)H_{int}(\tau)K_0(\tau,\tau')H_{int}(\tau')K_0(\tau',-\infty) + \cdots, \tag{12}$$

where in (12), the lowest order term is simply

$$K_0(t,t') = \exp[-iH_0(t-t')]. \tag{13}$$

In our model the electromagnetic coupling to the nuclear currents is mediated by the classical four-vector potentials A_μ. The source currents for these fields come from the motion of the nucleons, both collectively, and as motion within each nucleus. For definiteness, we consider a collision between two nuclei a and b, viewed in the equal velocity frame. The nucleus a moves with a velocity $+\beta$ parallel to the z-axis. The nuclei have charges Z_a and Z_b, respectively, and their trajectories are separated by an impact parameter, $\vec{b}$. Hereafter, in all equations, we employ natural units with $\hbar = c = m = e = 1$, m being the lepton mass. In presenting calculational results for physical observables, we restore the appropriate dimensional scaling. This is consistent with and facilitates comparisons with formulae in the literature [11]. In our units, each nucleus has a kinetic energy per nucleon, $E = M_N(\gamma - 1)$, given in terms of the Lorentz factor, $\gamma = (1-\beta^2)^{-1/2}$, and the

nucleon mass, M_N. The electromagnetic potential is the sum of the two terms coming from nuclei a and b, respectively

$$A^\mu(x) = A^\mu_a(x) + A^\mu_b(x)$$

with corresponding currents

$$\mathcal{J}^\mu(x) = \mathcal{J}^\mu_a(x) + \mathcal{J}^\mu_b(x).$$

The four-potentials are obtained from Maxwell's equations

$$\partial_\mu \partial^\mu A^\nu(x) - \partial^\nu(\partial_\mu A^\mu) = \mathcal{J}^\nu(x). \tag{14}$$

The development of these equations is straightforward; we work in the rest frame of each respective nucleus, solve for the four potentials in momentum space, and then Lorentz boost the result to the frame in which the collision is taking place. We shall specialize to spin-zero nuclei, and use time-reversal invariance; in the rest frame of a nucleus of charge Z

$$\begin{aligned} \mathcal{J}^0(Q) &= 8\pi^2 \delta(Q_0) Z f^Z(Q^2) G_E(Q^2) \\ \mathcal{J}^\mu(Q) &= 0 \qquad \mu \neq 0\,, \end{aligned} \tag{15}$$

where $f^Z(Q^2)$ is the momentum distribution of a proton in the nucleus, and $G_E(Q^2)$ is the electric distribution function of the proton. Details of this development are given in Ref. [13]. From (14) and (15), the four-vector potential associated with nucleus a is a function of the four-momentum Q, and in the center-of-momentum frame of the heavy ions, is given by

$$A^0_a(Q) = -8\pi^2 Z_a \gamma^2 \frac{\delta(Q_0 - \beta Q_z)}{Q^2} G_E(Q^2) f^{Z_a}(Q^2)\ \exp\left(i\vec{Q}_\perp \cdot \vec{b}/2\right)\,,$$

$$A_a^x(Q) = 0 \ , \tag{16}$$

$$A_a^y(Q) = 0 \ ,$$

$$A_a^z(Q) = \beta A_a^0(Q) \ .$$

The potentials from nucleus b can be easily obtained from (16) by the substitutions

$$\vec{b} \rightarrow -\vec{b}, \ \ \beta \rightarrow -\beta.$$

3. CROSS SECTIONS FOR PAIR PRODUCTION

If we focus on the second-order processes expressed by the diagram in Fig. 1, the relevant S-matrix element is given by

$$< k \mid S_{ab} \mid q > = (-i)^2 \int_{-\infty}^{\infty} d\tau \int_{-\infty}^{\tau} d\tau' < k \mid K_0(0,\infty) K_0(\infty,\tau)$$

$$\times \not{A}_a(\tau) K_0(\tau,\tau') \not{A}_b(\tau') K_0(\tau',-\infty) K_0(-\infty,0) \mid q >, \tag{17}$$

where

$$\mid q > = \mid \chi_q^{(-)} > , \mid k > = \mid \chi_k^{(+)} > , \tag{18}$$

and S_{ba} is obtained from S_{ab} by reversing the signs of the velocity β and the impact parameter $\vec{b}$.

The pair production cross section is given, adequately for the purposes in hand [11], by the expression

$$\sigma = \int d^2b \sum_{k>O} \sum_{q<O} |< k \mid S_{ab} + S_{ba} \mid q >|^2 \ . \tag{19}$$

The amplitude for the diagram in Fig. 1 was given in (17) and can be understood as follows:

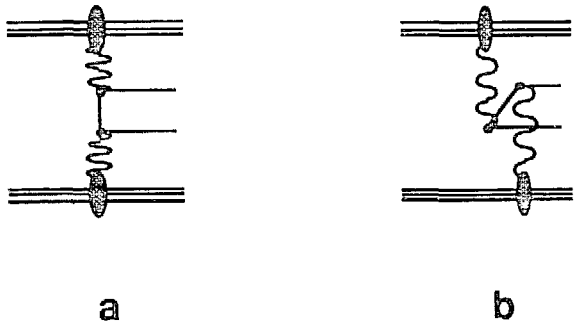

Fig. 1. Direct (a) and crossed (b) Feynman diagrams for pair production in a heavy-ion collision.

In the center-of- momentum frame of the colliding nuclei, the classical electromagnetic fields of the nuclei provide a source of "off-shell" photons with four momenta given as Q_a, and Q_b, respectively

$$Q_a = (\omega_a, \vec{Q}_{a\perp}, \frac{\omega_a}{\beta}) ,$$

$$Q_b = (\omega_b, \vec{Q}_{b\perp}, -\frac{\omega_b}{\beta}) . \tag{20}$$

The lepton and antilepton carry four-momentum k and q, respectively, and the total momentum of the pair

$$P = k + q . \tag{21}$$

The frequencies of the virtual photons are explicitly given by

$$\omega_a = \frac{E_k^{(+)} - E_q^{(-)} + \beta(k_z - q_z)}{2} ,$$

(22)

$$\omega_b = \frac{E_k^{(+)} - E_q^{(-)} - \beta(k_z - q_z)}{2}.$$

The photon and lepton part of the diagram follow the usual Feynman rules so that

$$P = Q_a + Q_b \ . \tag{23}$$

Thus with a modest amount of analysis, the amplitude (17) can be written as

$$< k \mid S_{ab} \mid q >= \frac{i}{\beta} \int \frac{d^2\tau_\perp}{(2\pi)^2} \exp(-i\vec{\tau}_\perp \cdot \vec{b}) F_a(Q_a^2) F_b(Q_b^2) \mathcal{T}_{kq} \left(\frac{\vec{P}_\perp - \vec{\tau}_\perp}{2} : \beta \right) \ , \tag{24}$$

where $\tau_\perp$ is the transverse momentum transfer

$$\vec{\tau}_\perp = \vec{Q}_{a\perp} - \vec{Q}_{b\perp}. \tag{25}$$

The transverse momentum is not fixed by the kinematics, but depends on the distribution of momenta carried in the classical fields. The form factor $F(Q^2)$ expresses the momentum dependence of the vertex on the nucleon and nucleus distributions and is obtained from (18) for either nucleus a or b as,

$$F(Q) = 4\pi Z f^Z(Q) G_E(Q^2). \tag{26}$$

The reduced Feynman amplitude $\mathcal{T}$ in (17) relates the coupling of the photon lines to the outgoing fermion lines in terms of a projection matrix for the intermediate fermion state

$$\mathcal{T}_{kq}(\vec{p_\perp} : \beta) = < u_{\sigma_k}^{(+)} \mid (1 - \beta\alpha_z) \frac{H_0(\vec{p}) + \omega}{H_0(\vec{p})^2 - \omega^2} (1 + \beta\alpha_z) \mid u_{\sigma_q}^{(-)} >, \tag{27}$$

where

$$H_0(\vec{p}) = H_\perp(\vec{p}_\perp) + p_z\alpha_z,$$

$$H_\perp(\vec{p}_\perp) = \vec{\alpha}_\perp \cdot \vec{p}_\perp + \gamma_0.$$

The four-momentum p is that carried by the intermediate lepton state in Fig. 1

$$p = (\omega, \vec{p}_\perp, p_z) \,, \tag{29}$$

whose components (ω, p_z) depend on β, as in (31) below. The momentum in intermediate states is composed of parts transverse and parallel to the motion of the heavy ions, $\vec{p} = \vec{p}_\perp + p_z \vec{e}_z$, and the frequencies ω_a and ω_b are related to the lepton energy ω through

$$\omega_a = E_k^{(+)} - \omega, \;\; \omega_b = \omega - E_q^{(-)}. \tag{30}$$

The frequencies and intermediate longitudinal momentum are thus determined as functions of β

$$\begin{aligned} p_z(\beta) &= \frac{-E_k^{(+)} + E_q^{(-)} + \beta(k_z + q_z)}{2\beta} \\ \omega(\beta) &= \frac{E_k^{(+)} + E_q^{(-)} - \beta(k_z - q_z)}{2}. \end{aligned} \tag{31}$$

Utilizing the above analysis, the expression for the cross section (19) becomes,

$$\sigma = \frac{1}{4\beta^2} \sum_{\sigma_k, \sigma_q} \int \frac{dk_z dq_z d^2 P_\perp}{(2\pi)^4} \int \frac{d^2 Q_{a\perp} d^2 Q_{b\perp}}{(2\pi)^4}$$

$$\times \mid F_a(Q_a^2) F_b(Q_b^2) \mid^2 \mid \mathcal{T}_{kq}(\frac{\vec{P}_\perp - \vec{\tau}_\perp}{2} : \beta) + \mathcal{T}_{kq}(\frac{\vec{P}_\perp + \vec{\tau}_\perp}{2} : -\beta) \mid^2 . \tag{32}$$

The expression (32) will be evaluated, without further approximation, using the Monte Carlo technique described in the next section.

4. MONTE CARLO INTEGRATION

The evaluation of (32) entails the integration of a positive function over eight variables. We can transform all of the integration into new variables which span the interval $(0,1)$, as follows. The rule, which greatly simplifies the numerics, is to scale all longitudinal momenta by the Lorentz factor associated with the collisions. Thus we map the coordinates (k_z, q_z) onto a vector, $\vec{\kappa}$, so that

$$\int_{-\infty}^{\infty} dk_z \int_{-\infty}^{\infty} dq_z = \int_0^{\infty} \kappa d\kappa \int_0^{2\pi} d\phi_\kappa \ . \tag{33}$$

The magnitude of the vector κ is scaled by the Lorentz factor γ associated with the collision. The integration over $\vec{P}_\perp$ is given as

$$\int d^2 P_\perp = \int_0^{P_u} P_\perp dP_\perp \int_0^{2\pi} d\phi_\perp \ . \tag{34}$$

The integration on the magnitude of $P_\perp$ is scaled with the mass of the lepton and is carried out with a simple quadrature formula, thus effectively mapping the integration onto the interval $(0, P_u)$. The integration on the transverse momenta of the two photons is given by the following transformation which is applied equivalently to both a and b.

$$\int d^2 Q_\perp = C \int_0^{\pi/2} d\theta \tan\theta \int_0^{2\pi} d\phi \ , \tag{35}$$

where the constant C is the frequency carried by the field associated with either nucleus a or b, given in (22),

$$C = \omega/\gamma \ .$$

Thus we can transform (32) in terms of an eight-fold integration over a unit hypercube having the form

$$\sigma = F_0 \int_0^1 dx_1 dx_2 \cdots dx_8 f(x_1, x_2, \cdots, x_8) \,, \tag{36}$$

where F_0 is chosen so that $f \leq 1$, and where the coordinates $\{x_i\}$ are simply related to the set $\{\kappa, \phi_\kappa, P_\perp, \phi_\perp, \theta_a, \phi_a, \theta_b, \phi_b\}$. At this point there are several different ways to proceed. We shall discuss two approaches that are equally successful.

Method 1

In the present case we have found it necessary to start with an estimate F_0, which is periodically improved by noting the largest value of f for varying numbers of Monte Carlo points. The algorithm proceeds by making *throws* in a nine-dimensional space, $\vec{y} = \{y_1, \ldots, y_9\}$, where $0 < y_j < 1$. We then calculate

$$x_9 = f(y_1, y_2 \cdots, y_8), \tag{37}$$

so that x_j lies in the range $0 < x_j < 1$. The *throw* is said to be *successful* if $x_9 > y_9$. After T throws, let the number of successes be S. The cross section is given by

$$\sigma = F_0 \frac{S}{T} \,, \tag{38}$$

with a proportional error in σ / F_0 of

$$\Delta = \left(\frac{1}{S} + \frac{1}{T} \right)^{\frac{1}{2}} . \tag{39}$$

Clearly, a good estimate of F_0 is desirable. We are able to compensate for the lack of *a priori* knowledge of F_0 by analysing each throw for a set of F_0 in parallel. At

the end of a run, the estimates of σ thereby obtained from (38) were interpolated to the best value of F_0 inferred from the run itself. The improved value of F_0 was used in subsequent runs. In Fig. 2 we display the error Δ as a function of the number of Monte Carlo points for a test run, $\Delta \simeq 30 - 100/T^{\frac{1}{2}}$.

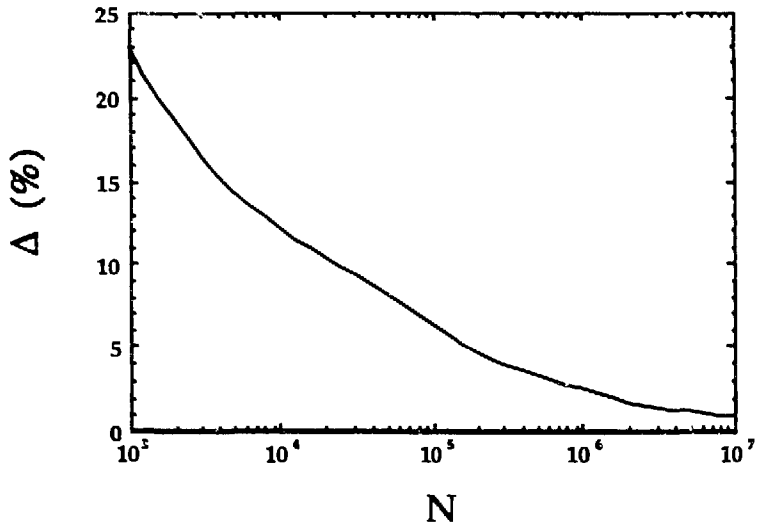

Fig. 2. Percentage error in Monte Carlo integration, Δ, vs. the number of Monte Carlo points, N.

We observe a rapid and stable convergence of the sampling algorithm as described above. Typical success rates were $S/T \simeq 10^{-3} - 10^{-4}$.

Method 2

In this approach, an eight-fold integration on the unit hypercube is approximated by a *sampling* of the integrand T times and then taking

$$\sigma = \frac{F_0}{T} \sum_{i=1}^{T} f(x_1(i), x_2(i), \cdots, x_8(i)) \ , \tag{40}$$

where the set $\{x_1(i), x_2(i), \cdots, x_8(i)\}$ denotes the ith sampling of the coordinates. If these variables are uniformly distributed on the interval $(0, 1)$, then (40) is just the

Stiltjes definition of integration. Here, a single sampling of the coordinates requires eight independent pseudo-random numbers. Each evaluation of the function f can be thought of as a statistical estimate of σ/f_0 with a corresponding variance. Thus, after T throws, the corrsponding error works out to be

$$\Delta_T^2 = \frac{1}{T}\sum_{i=1}^{T}(f(x_1(i), f_2(i), \cdots, x_8(i)) - \sigma/F_0)^2 \,, \tag{41}$$

so that both the cross section and its variance can be computed at the same time. In both methods the error goes as $1/\sqrt{T}$. This rate of convergence may seem slow compared to the more sophisticated prescriptions utilizing Gauss points; for example, using K^{th} order Gauss–Laguerre integration, the error goes as $\Delta_G = 1/T^{2K-1}$. However, in eight dimensions, the overall error goes as $\Delta_G^{1/8}$ so that Monte Carlo wins. Generally, any calculation is a balance between accuracy and economy; we summarize some of the features of Monte Carlo calculations which we find advantageous.

- Both of the above Monte Carlo algorithms are basically very simple to use without a great deal of specialized knowledge, and both methods vectorize easily on supercomputers. Thus modern calculations can be effected with a large number of integration points.

- Very complicated constraints can be placed on the summations, therby allowing experimental "cuts" on phase space to be directly calculated. This is explored in depth in the section on $\pi^- p$ collisions.

- The integration can be "binned" in terms of other variables during the evaluation. Thus a variety of distributions can be directly computed without the need for calculating difficult Jacobians.

- We are basically studying two-photon diagrams which entail eight independent integrations. Diagrams of much higher order can be evaluated with this approach. Although not discussed in these lectures, we have also examined the radiative corrections to pair production, which reduces to a ten dimensonal problem.

In the following two sections we shall discuss two very different application of these techniques.

5. μ, τ PAIR PRODUCTION

In this section we study the effects of the nuclear form factors on the μ and τ pair production. In particular, we consider the symmetric collision of two gold nuclei at RHIC energies. From (18), the charge current distribution in the gold nucleus involves the product of the momentum distribution of a proton in the nucleus, f^Z, times the electric distribution function of the proton, G_E. For small values of the momentum transfer, f^Z and G_E are related to the Fourier transforms of the gold and proton charge distributions, respectively. However, for large values of Q^2, these are difficult to determine experimentally [14]. Theoretical and empirical models, as for example, perturbative QCD [15], vector meson dominance [16], and dimensional scaling [17] give predictions at large Q^2 which seem to agree with

the measured values of the magnetic form factor [14]. Experimental tests of these predictions for the electric form factor are presently unavailable.

Accordingly, we have chosen empirical form factors for both the proton and the Au nucleus. For Au, we employ a Fermi function with two parameters, which are adjusted to fit low-energy elastic electron scattering data [18]. This is shown in Fig. 3 as the solid curve.

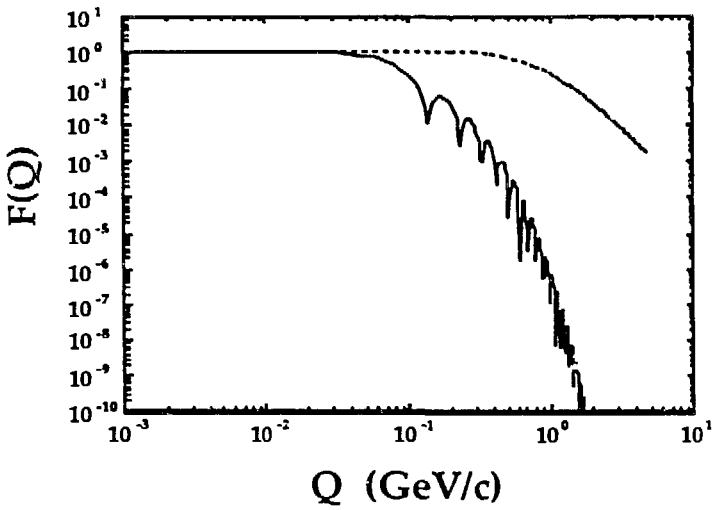

Fig. 3. The proton (dashed curve) and Au (solid curve) form factors as a function of the magnitude of the photon four momentum in units of GeV/c.

The proton form factor is assumed to have a dipole form [13] given by

$$G_E(Q^2) = \left(1 + \frac{Q^2}{\Lambda_p^2}\right)^{-2} \quad , \quad \Lambda_p^2 = 0.71 \mathrm{GeV}^2/\mathrm{c}^2 \, . \tag{42}$$

This function is depicted as the dashed curve in Fig. 3. These curves illustrate, in a simple way, that the electromagnetic vertex is strongly suppressed for values of Q^2 greater than about one $\mathrm{GeV}^2/\mathrm{c}^2$.

In Fig. 4 we present lepton pair cross sections calculated for colliding beams of

Au nuclei at a bombarding energy per nucleon of 100 GeV. Here, we give the total cross section in units of σ_0

$$\sigma_0 = \frac{(Z\alpha)^4 \hbar^2}{M_\ell^2 c^2} \tag{43}$$

as a function of the intrinsic mass of the lepton, M_ℓ, treated as a continuous variable. Thus, there are only three physical masses in the figure, 5.11×10^{-4}, 1.06×10^{-2}, and 1.784 GeV/c^2, corresponding to the electron, muon, and tauon respectively. The dotted curve represents results obtained with point charge nuclei, the dashed curve results obtained with the proton form factor, and the solid curve results obtained with form factors for the proton and for the Au nucleus included. We note that for masses less than about 10 MeV/c^2, neither the proton nor the Au form factor substantially affects the cross section. Thus, the total electron pair production is not strongly affected by the details of the nuclear currents. However, for values of the mass near about 2 GeV/c^2, the results with the proton form factor are more than an order of magnitude smaller than the corresponding point charge results, and the results which include the Au form factor are reduced by more than a factor of 10^3. Hence, tauon pair production is extremely sensitive to these form factors. The muon pair cross sections are suppressed by about a factor of four compared to the results with point nuclear currents.

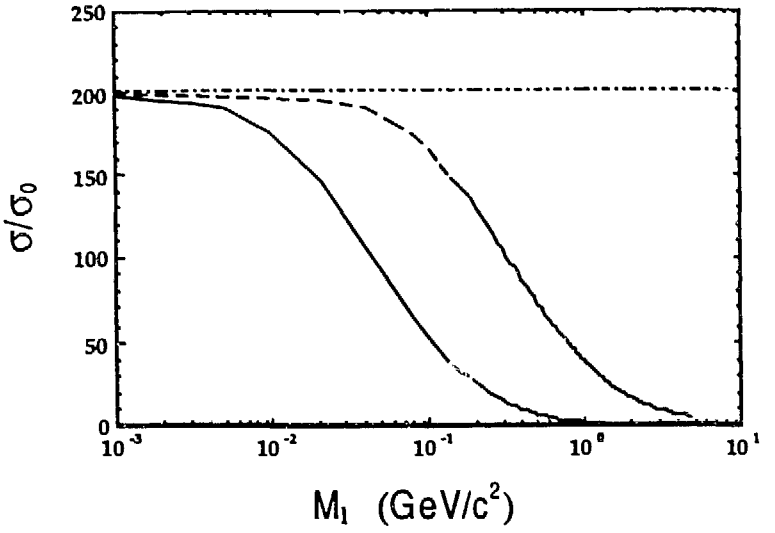

Fig. 4. Dependence of pair production cross sections on the intrinsic lepton mass M_ℓ for collisions of $Au + Au$ at 100 GeV per nucleon. The ratio of the cross section to the reduced cross section σ_0 is plotted vs. M_ℓ. Full line: result including Au and proton form factors; dashed line: result including only the proton form factor; dotted line: point source result.

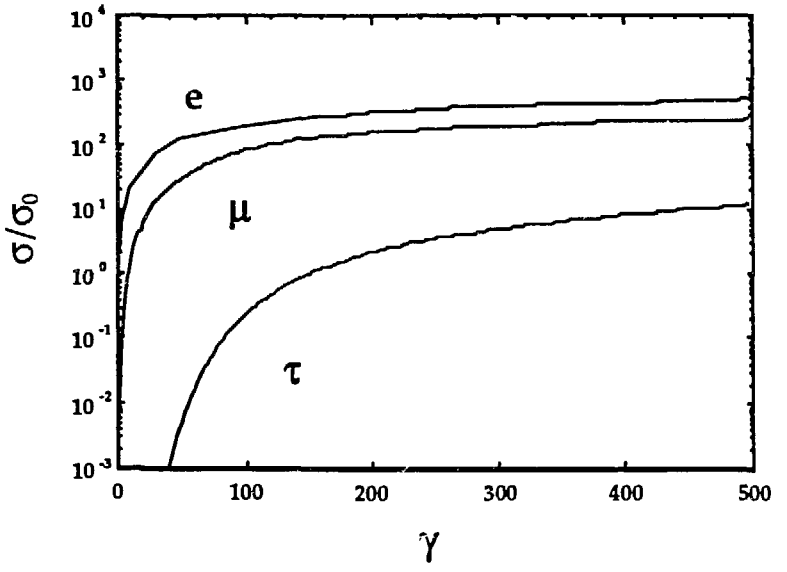

Fig. 5. The pair cross sections for colliding beams of Au nuclei as a function of the Lorentz γ of the beam. The reduced cross section σ_0 is defined in (43). Full line: electrons, dashed line: muons, long dashed line: tauons.

A comparison of the electron, muon, and tauon total cross sections as a function

of the Lorentz γ of the beams is given in Fig. 5 for collisions of Au nuclei. These results include both nuclear form factors as described previously. Note that the results for the electrons are equivalent to the same results using point nuclear currents. Values of γ about 3 and 10 approximately correspond to experiments at the AGS and at CERN. Here we see that for all practical purposes, the form factors completely suppress the tauon cross sections and reduce the muon cross sections by more than a factor of 100 at $\gamma = 10$. Thus it is only at the highest bombarding energies, such as will be attained at RHIC, that heavy leptons are produced with large multiplicities. These results are summarized in Table 1.

Table 1

Results for the coherent muon and tauon pair production for 100 GeV per nucleon colliding beams of Au nuclei.

	μ (mb)	τ (mb)
Point Source	770	2.7
Form Factor	200	2.8×10^{-3}

The role of the nuclear form factors in heavy lepton production can be understood in greater depth by examining their effects on the pair distributions in rapidity, transverse momentum, and invariant mass. These are shown in Figs. 6, 7, and 8, for muons.

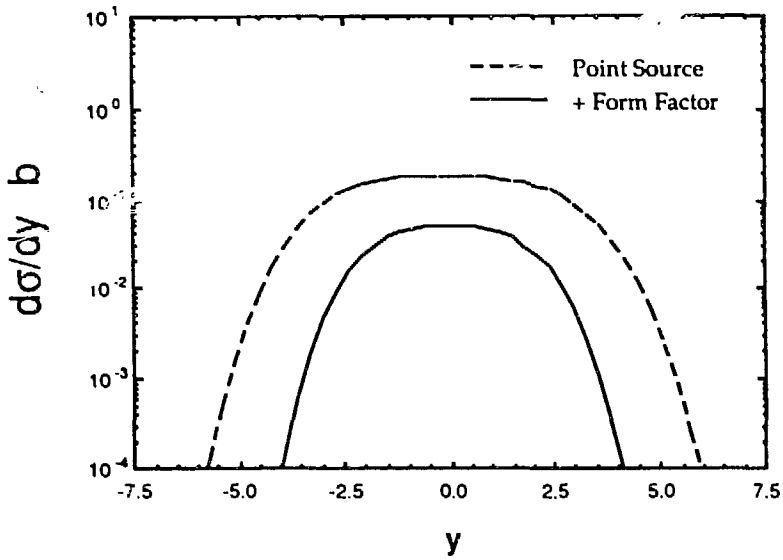

Fig. 6. Rapidity distribution of dimuons produced from colliding beams of Au nuclei at an energy per nucleon of 100 GeV. The solid curve is the calculated result including the proton and Au form factors, and the dashed curve is the result from point charge nuclei.

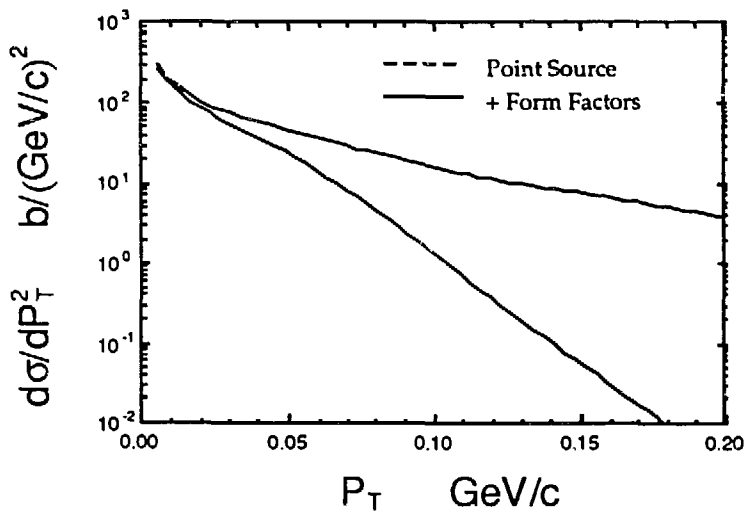

Fig. 7. Transverse momentum distribution of dimuons produced from colliding beams of Au nuclei at an energy per nucleon of 100 GeV. The solid curve is the calculated result including the proton and Au form factors, and the dashed curve is the result from point charge nuclei.

Again, we are considering colliding beams of Au nuclei at 100 GeV per nucleon.

In Fig. 6 we show the μ pair cross section as a function of the rapidity. The solid curve gives the results which include the nuclear form factors, and the dashed curve gives the results for point nuclear currents. The rapidity of the Au beams is approximately $Y = \pm 5.29$. Again, we are considering colliding beams of Au nuclei at 100 GeV per nucleon. In Fig. 6 we show the μ pair cross section as a function of the rapidity. The solid curve gives the results which include the nuclear form factors, and the dashed curve gives the results for point nuclear currents. The rapidity of the Au beams is approximately $Y = \pm 5.29$. Thus we observe that the form factors reduce the cross section by about a factor of ten and result in a distribution which is sharply confined to the region of central rapidity. In Fig. 7 the distribution in transverse momentum, P_T, is compared for the two cases. We note that the two curves are approximately the same for values of P_T near zero. The Compton momentum of the μ is about 0.1 GeV/c; at this value of P_T the nuclear form factors have reduced the cross section by an order of magnitude, and hence the resulting distribution is concentrated at small values of P_T. The distribution as a function of the invariant mass is shown in Fig. 8. Again we are comparing the results of calculations with form factors and with point currents. In this case the threshold for the mass distribution is about 0.2 GeV/c^2, and we see a strong reduction in the distribution due to the form factors. For τ pair production, these effects are even more pronounced.

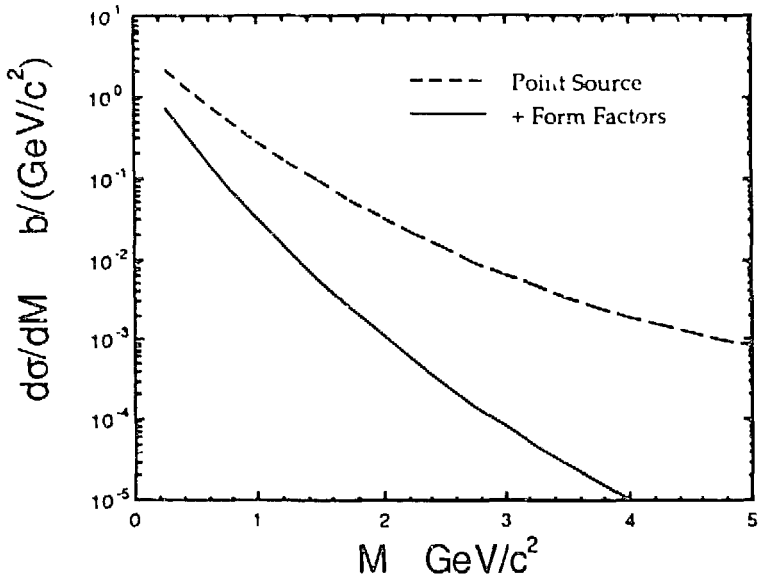

Fig. 8. Invariant mass distribution of dimuons produced from colliding beams of Au nuclei at an energy per nucleon of 100 GeV. The solid curve is the calculated result including the proton and Au form factors, and the dashed curve is the result from point charge nuclei.

6. $\pi^- P$ COLLISIONS

The emission of electron–positron pairs has been observed [9,10] in π^- p collisions with corresponding pion momenta of 16 and 17 Gev/c. The experiments detected pairs over a limited range of invariant pair mass, given by $0.2 \leq M \leq 1.2$ GeV/c^2. A large peak near $M = 0.8$ GeV/c^2 was observed. This peak is well understood as resulting from the direct electromagnetic decay of the ρ and ω mesons, $\rho \rightarrow e^+ e^-$, and $\omega \rightarrow e^+ e^-$. A continuum of pairs is also seen at lower invariant masses. These pairs were deemed anomalous, as conventional hadronic mechanisms failed to explain the data. We demonstrate here that an *ab initio* calculation of the two-photon mechanism produces results that are in quantitative agreement with

the continuum data.

The experimental results of Refs. [9] and [10] are shown in Figs. 9, 10, and 11. The qualitative features of the cross sections are clear. The cross section decreases with increasing pair mass, decreases with increasing Feynman x (defined as the total longitudinal momentum of the pair divided by the maximum value allowed kinematically), and decreases with increasing transverse momentum.

If we calculate the two-photon process in the limit where the relative motion of the pion and proton is treated classically [19], the total cross section for electron–positron pair production is given by (19). For a 17 GeV/c pion, we can use a straight-line trajectory. The scattering amplitude has the two terms corresponding to crossed and uncrossed photons as shown in Fig. 1 and as discussed in Section 2. Here $A_a^\mu(q)$ and $A_b^\mu(q)$, which appear as prescribed external fields, are given by the photon propagator times the matrix element of the proton or pion current, as given in (15) and (16). However, the resulting expression for the proton current is incomplete. The most general form of the electromagnetic current of the proton is [13]

$$J^\mu(p'\sigma', p\sigma) = e\,\overline{u}^{(\sigma')}(p')\,[\gamma^\mu\, F_1(p'-p)]\,u^{(\sigma)}(p)$$
$$-\frac{e}{2M_p}\,\overline{u}^{(\sigma')}(p')\,[\sigma^{\mu\nu}(p'_\nu + p_\nu)\,\kappa\, F_2(p'-p)]\,u^{(\sigma)}(p)\,. \qquad (44)$$

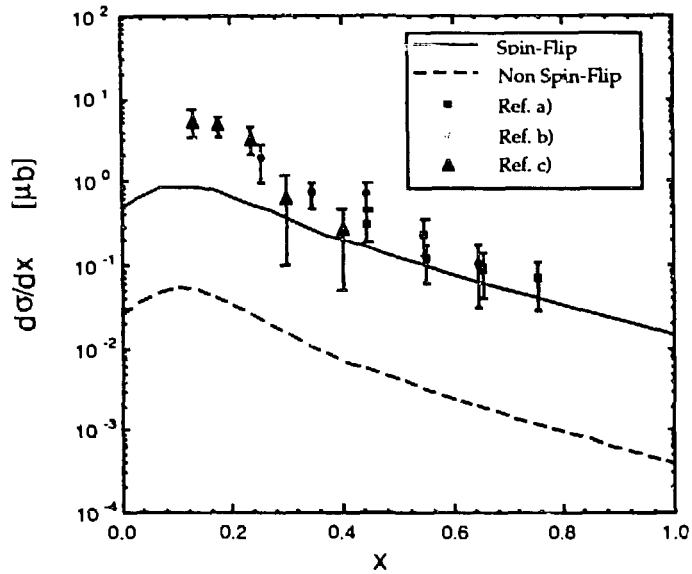

Fig. 9. The differential cross section for electron–positron pair production *vs.* Feynman x. The dashed curve is the result omitting the spin-flip terms. The data are from Ref. [9].

By inserting explicit expressions for the proton spinors in (44) and multiplying by the photon propagator, the vector potential from the proton in (16) becomes

$$A_a^\mu(\mathbf{b};q) = a^\mu(\mathbf{b}:q) + \delta a^\mu(\mathbf{b}:q)\ ,$$

where the term which corresponds to non-spin-flip events is

$$a^o(\mathbf{b}:q) = 2\pi\, e\, \delta(q_o - \beta q_z)\, \gamma\, \frac{e^{-i\vec{q}\cdot\vec{b}/2}}{q_z^2 + \gamma^2 q_\perp^2}\, G_E(q^2)\ ,$$

$$a^x(\mathbf{b}:q) = 0\ ,\quad a^y(\mathbf{b}:q) = 0\ ,\quad a^z(\mathbf{b}:q) = \beta\, a_o^{(+)}(\mathbf{b}:q)\ . \tag{45}$$

The electric form factor of the proton is given in (42) [13]. The second term in

$A_a^\mu(q)$, which involves both $F_1(q)$ and $F_2(q)$, corresponds to events in which the proton spin flips. This term yields

$$\delta a^x(\mathbf{b}:q) = 2\pi \frac{e}{2M_p}\delta(q_o - \beta\, q_z)\, \frac{e^{-i\vec{q}\cdot\vec{b}/2}}{q_z^2 + \gamma^2 q_\perp^2}\, q_z\, G_M(q^2)\ ,$$

$$\delta a^y(\mathbf{b}:q) = 2\pi \frac{e}{2M_p}\delta(q_o - \beta\, q_z)\, \frac{e^{-i\vec{q}\cdot\vec{b}/2}}{q_z^2 + \gamma^2 q_\perp^2}\, i\, q_z\, G_M(q^2)\ ,$$

$$\delta a^z(\mathbf{b}:q) = -2\pi \frac{e}{2M_p}\delta(q_o - \beta q_z)\, \gamma\, \frac{e^{-i\vec{q}\cdot\vec{b}/2}}{q_z^2 + \gamma^2 q_\perp^2}\, (q_x + iq_y)\, G_M(q^2)\ ,$$

$$\delta a^o(\mathbf{b}:q) = \beta\, \delta a_o^{(+)}(\mathbf{b}:q)\ , \tag{46}$$

where the magnetic form factor of the proton, $G_M(q^2)$, is normalized so that $G_M(0) = 1+\kappa = 2M_p\mu_p/e$, where μ_p is the magnetic moment of the proton. We use the same dipole form for the magnetic form factor, $G_M(q^2) = (1+\kappa)(1+q^2/\Lambda_p^2)^{-2}$, as for $G_E(q^2)$. For the spin-zero pion the electromagnetic current is given by

$$J^\mu(p',p) = e\,(p'^\mu + p^\mu)\, G_F\left((p'-p)^2\right)\ . \tag{47}$$

which produces a similar result for $A_b^\mu(q)$ as is given in (16); in the center-of-velocity frame, $A_b^\mu(q)$ is given by (45) with $\beta \to -\beta$ and $\mathbf{b} \to -\mathbf{b}$. We utilize a monopole form for the electric form factor of the pion, $G_E(q^2) = (1 + q^2/\Lambda_\pi^2)^{-1}$, where $\Lambda_\pi^2 = 0.59$ GeV^2/c^2 [13]. The expression derived here for the total cross section is Lorentz invariant and is most easily evaluated in the center-of-velocity frame. Finally, the crossed photon term, which contributes to (19), is added coherently to the direct term.

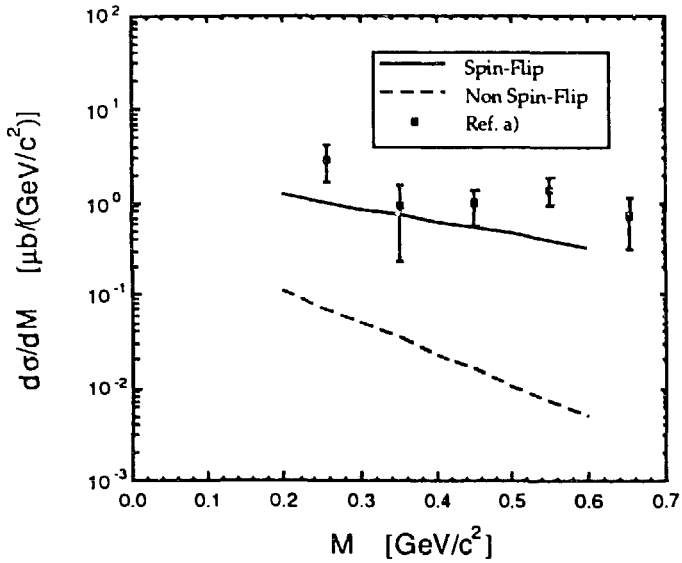

Fig. 10. The differential cross section for electron–positron pair production *vs.* the pair mass. The dashed curve is the result omitting the spin-flip terms. The data are from Ref. [9].

In summary, we take the classical limit on the relative motion of the proton and pion of standard QED perturbation theory for the two–photon process. The arguments of Ref. [19] indicate that the wavelength of the relative pion-nucleon motion is sufficiently large and the electromagnetic field sufficiently smooth that we are well into the classical region. In this region, the matrix element of the current, which couples the proton or the pion to the electromagnetic field multiplied by the photon propagator, takes the form of prescribed electromagnetic fields that have been boosted from the rest frame to a frame with velocity $-\beta$, as given in (45) for the non-spin-flip term, and (46) for the spin-flip term.

The eight-dimensional integration required to calculate the total cross section in

(32) is done utilizing the Monte Carlo technique described earlier. We impose on the Monte Carlo integration the experimental cut on the pair mass, $0.2 \leq M \leq 0.8$ GeV/c^2. Points which correspond to invariant masses outside this region are counted in the overall normalization of the calculation, but do not contribute to the data of present interest, and thus the integrand need not be calculated for these points. The total cross section for electromagnetic pair production is about 55 μb, of which only 0.5 μb lies within the cut. The differential cross sections follow simply by binning the points as a function of the relevant independent variable.

The results of a calculation which used about 25×10^6 Monte Carlo points are shown in Figs. 9-11. The contributions which arise from the non-spin-flip current, (45), are presented as the dashed curves. These results are significantly below the data. The cross sections for production from the currents given in (45) are large [11] for small electron and positron momenta. However, in the kinematical region imposed by the cut on the invariant mass, this process produces a very small cross section. In addition, the direct and crossed terms interfere destructively to reduce the predicted cross sections by two orders of magnitude.

The contributions for electron–positron pair production, including the magnetic spin-flip term, (46), are also shown in Figs. 9-11 as the solid curve. We see that the results are in reasonable agreement with the data. We stress that the calculation is made *ab initio* with no adjustable parameters. Although the overall agreement is good, the cross sections in Fig. 9 lie a little below the data for low Feynman x. This may be due to our use of the lower cut on the invariant mass at exactly

0.2 GeV/c^2. If we decrease this value slightly, the cross sections at low x and low $p_\perp$ are enhanced. The difficulty might also lie in our neglect of the final-state distortions of the electron and positron. The cross sections for the slower-moving leptons might well be somewhat higher if distorted waves were used.

The spin-flip term, (46), is of order q/M_p, as compared to the leading term, (45). The reduction due to this factor is more than compensated for by two features of the spin-flip current: 1) the current has transverse components, and 2) the 0 and z components are proportional to the transverse momentum of the photon. Thus the spin-flip current produces pairs at the large values of transverse momentum emphasized by the experimental cut on the invariant mass.

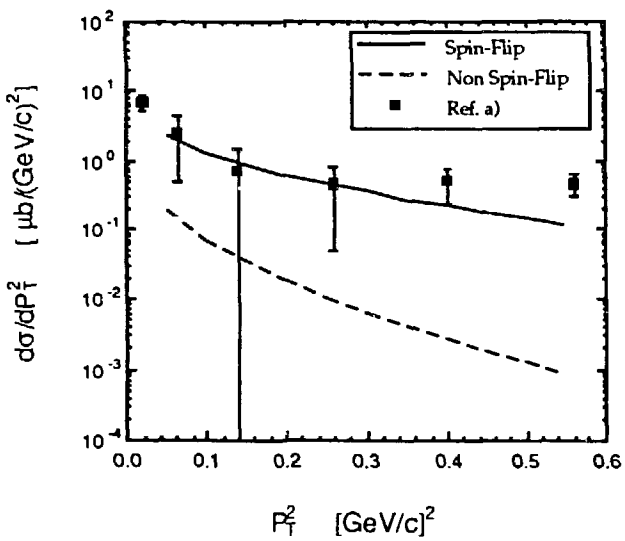

Fig. 11. The differential cross section for electron–positron pair production *vs.* the transverse momentum of the pair. The dashed curve is the result omitting the spin-flip terms. The data are from Ref. [9].

We conclude from the general quality of the agreement of the calculation with the data that the lepton pairs observed in Refs. [9] and [10] are produced, to a

large extent, via the two-photon mechanism specifically by the magnetic part of the proton current. The calculation itself allows some internal consistency checks on this view of the physics. The presence of the proton and pion form factors reduces the predicted cross sections by less than a percent. This indicates that the cross section arises from a region where the scale for the momentum or energy of the virtual photon is given by several hundred MeV or less. At these momentum transfers, the dominant response of the proton or the pion is the coherent elastic response, although the excitation of the nucleon to a delta, or the pion to a rho might also contribute a non-negligible amount in this kinematic region. We note that the coincidence data given in Ref. [10] are consistent with this low multiplicity interpretation of the data. This relatively low momentum transfer from the hadrons does not justify a quark level calculation of the two-photon process, as was done in Ref. [10]. We further point out that the independent quark-level processes are suppressed by a factor of $Z_1^2\, Z_2^2$, with Z_i the charge of the quark, and thus can only become the dominant term in kinematic regions where the elastic form factor suppresses the coherent elastic term. In our calculation we integrate over impact parameters starting at zero. For impact parameters less than one Fermi, the pion and proton will undergo strong interactions which would invalidate the pure electromagnetic calculation done here. However, we find that non-negligible numbers of lepton pairs are emitted out to impact parameters of greater than one hundred Fermis. Thus, neglecting the contribution which arises from impact parameters below one Fermi would have little effect on our results.

Electromagnetic lepton pair production in particle collisions is important for several reasons. It is well understood that the two-photon process can produce large numbers [5,11] of soft pairs. Here we have found that it can also produce pairs with significant transverse momentum, which could provide a background for the lepton pairs emitted in heavy-ion collisions. If the lepton pairs are to serve as a probe of the quark-gluon plasma, this background must first be understood. Also, the Lorentz-contracted fields, represented by the vector potentials of (45) and (46), become very large for the ultrarelativistic heavy ions that will be produced at RHIC and perhaps at the SSC. In this case, the perturbative approach utilized here will certainly be inadequate. Lepton production would then offer the opportunity to study QED in a region where it is not perturbative. The present results are needed as a baseline for this study.

7. CONCLUSIONS

We conclude by reviewing the questions raised in the Introduction concerning electromagnetic mechanisms for pair production. The present work supplies detailed information on the backgrounds necessary to interpret analysis of heavy-ion dimuon data. We have shown that muon production in heavy-ion collisions is largely coherent over distances of the dimension of the nucleus. In the case of tauons, the form factors break this coherence. The same result should be true for even more massive particles such as W-pairs. Thus it is expected that the incoherent production will dominate the two-photon mechanism for particles as massive

as the tauon or W. In summary:

- We have calculated heavy lepton pair production in the two-photon approximation. We have employed Feynman perturbation theory to go beyond equivalent photon formulations, and in particular, to incorporate correctly the transverse momentum dependence.

- We have shown that form factors must be included in calculations of muon and tauon pair cross sections. We employed the best fits to the elastic electron nucleus scattering data that presently exist. This determines the form factor for Q^2 less than about one $\mathrm{GeV}^2/\mathrm{c}^2$. There are no form factor data for heavy nuclei at larger values, and the sensitivity of the cross sections to the form factor in this region is not known. We note that other models, which fit the electron scattering data less well, differ in their cross section predictions by as much as a factor of ten. Thus, these effects need to be explored in greater depth.

- There is a need for measurements which will test theories of two-photon pair production and its scaling with charge, mass, and energy. If these issues are settled, the two-photon pair production could be a method of probing the form factors of heavy nuclei at large values of momentum transfer.

Our future work will address incoherent mechanisms, the effects of inelastic structure functions, and central collisions.

8. ACKNOWLEDGEMENTS

This research was sponsored by the Division of Chemical Sciences, Office of Basic Energy Sciences, and by the Division of Nuclear Physics of the U.S. Department of Energy under contract No. DE-AC05-84OR21400 with Martin Marietta Energy Systems, Inc.

REFERENCES

1. H. Gould, in "Proceedings of the Atomic Theory Workshop on Relativistic and QED Effects in Heavy Atoms", AIP Conf. Proc. 136, p. 66, (AIP, New York, 1985).

2. C. Bottcher and M.R. Strayer, in "Physics of Strong Fields", edited by W. Greiner, (Plenum, New York, 1987), Vol.153, page 629.

3. C. Bottcher and M.R. Strayer, "Proceedings of the Second Workshop on Experiments and Detectors for the RHIC", Berkeley, California, May 25-29, 1987, page 279, (LBL-24604).

4. G. Bauer and C.A. Bertulani, Phys. Rev. C35, 836 (1987).

5. C. Bottcher and M.R. Strayer, Nucl. Inst. and Meth. B31, 122 (1988).

6. E. Teller, Nucl. Inst. and Meth. B24, 1 (1987).

7. Elena Papageorgiu, Phys. Rev. D40, 92 (1989); Nucl. Phys. A498, 593c (1989); M. Drees, J. Ellis and D. Zeppenfeld, Phys. Lett. 223b, 454 (1989).

8. M. Grabiak, B. Müller, W. Greiner, G. Soff, and P. Koch, J. Phys. G15, L25 (1989); G. Soff, J. Rau, M. Grabiak, B. Müller and W. Greiner, *Production of super-symmetric particles and Higgs bosons in ultrarelativistic heavy-ion collisions*, Preprint,1989, (GSI-89-55); J. Rau, M. B. Müller and W. G. Soff, *Production of super-symmetric particles in ultrarelativistic heavy-ion collisions*, Preprint, submitted to J. Phys. G, 1989 (GSI-89-76).

9. R. Stroynowski, D. Blockus, W. Dunwoodie, D. W. G. S. Leith, M. Marshall, C. L. Woody, B. Barnett, C. Y. Chien, T. Fiefuth, M. Gilchriese, D. Hutchinson, W. B. Johnson, P. Kunz, T. Lasinski, L. Madansky, W. T. Meyer, A. Pevsner, B. Ratcliff, P. Schacht, J. Scheid, S. Shapiro and S. Williams, Phys. Lett. **97B**, 315 (1980); D. Blockus, W. Dunwoodie, D. W. G. S. Leith, M. Marshall, R. Stroynowski, C. L. Woody, B. Barnett, C. Y. Chien, T. Fieguth, M. Gilchriese, D. Hutchinson, W. B. Johnson, P. Kunz, T. Lasinski, L. Mandansky, W. T. Meyer, A. Pevsner, B. Ratcliff, P. Schacht, J. Sheid, S. Shapiro and S. Williams, Nucl. Phys. **B201**, 205 (1982).

10. J. Stekas, G. Abshire, M. R. Adams, C. Brown, L. Cormell, E. Crandall, G. J. Donaldson, J. Goldberger, H. A. Gordon, P. D. Grannis, B. T. Meadows, G. R. Morris and P. Rehak, Phys. Rev. Lett. **47**, 1686 (1981); M. R. Adams, G. Abshire, C. Brown, E. S. Crandall, J. Goldberger, P. D. Grannis, B. T. Meadows, J. Stekas, G. J. Donaldson, H. A. Gordon, G. R. Morris, P. Rehak and L. Cormell, Phys. Rev. D. **27**, 1977 (1983).

11. C. Bottcher and M.R. Strayer, Phys. Rev. D39, 1330 (1989).

12. C. Bottcher, M.R. Strayer, C. J. Albert and D.J. Ernst, to appear in Phys. Lett. B, 1990.

13. F.E. Close, "An Introduction to Quarks and Partons", (Academic Press, New York, 1979).

14. R.C Walker, B.W. Filippone, J. Jourdan, R. Milner, R. Mc Keown, D. Potterveld, R. Arnold, D. Benton, P. Bosted, G. de Chambrier, L. Clogher, A. Lung, S.E. Rock, Z.M. Szalata, A. Para, F. Dietrich, K. Van Bibber, J. Button-Shafer, B. Debebe, R.S. Hicks, S. Dasu, P. de Barbaro, A. Bodek, H. Harada, M.W. Krasny, K. Lang, E.M. Riordan, J. Alster, R. Gearhart, L.W. Whitlow, OAP-697, March, 1989, submitted to Phys. Lett . B.

15. G.P. Lepage and S.J. Brodsky, Phys. Rev. Lett. 43, 545 (1979).

16. F. Iachello, A.D. Jackson, and A. Landé, Phys. Lett. 43B, 191 (1973).

17. S.J. Brodsky and G. Farrar, Phys. Rev. D11, 1309 (1975).

18. Nuclear Data Tables, 14 (1974).

19. A. S. Umar, M. R. Strayer, D. J. Ernst, and K. R. Sandhya Devi, Phy. Rev. C 30, 1934 (1984).